ACS OMEGA

http://pubs.acs.org/journal/acsodf

Article

Theoretical Study on the Unimolecular Pyrolysis of Thiophene and Modeling

Tianshuang Li, Hongliang Zhang, Yun Li,* Jie Li,* Jingkun Wang, and Jin Xiao

Cite This: *ACS Omega* 2021, 6, 20471−20482

Read Online

ACCESS | Metrics & More | Article Recommendations | Supporting Information

ABSTRACT: Thiophenic sulfur is the most stable and abundant organic sulfur species in petroleum. Removal of thiophenes has profound significance in environmental protection. In this work, we investigate the unimolecular pyrolysis of thiophene from a kinetic perspective. High-level ab initio methods have been employed to deduce the potential energy surface. Rate coefficients of the elementary reactions are computed using variational transition-state theory at the CCSD(T)/CBS level to develop a kinetic model. By comparison with preceding experimental results, the kinetic model shows good performance in calculating the thiophene pyrolysis rate. The Arrhenius expression for thiophene unimolecular pyrolysis has been redetermined as $k = 1.21 \times 10^{13} \times \exp[(78.96\ \text{kcal/mol})/(RT)]$. The unimolecular pyrolysis of thiophene is mainly initiated by the ring-H migrations, whereas the C−S bond rupture has limited contribution to the overall pyrolysis rate. Thioketene (SC_2H_2) and ethyne (C_2H_2) are the major pyrolysis products at all temperatures. Significant amounts of the thioformyl (HCS) radical and CS could also be yielded. By contrast, atomic sulfur and H_2S are difficult to be directly produced. Possible secondary reactions in the products have also been discussed.

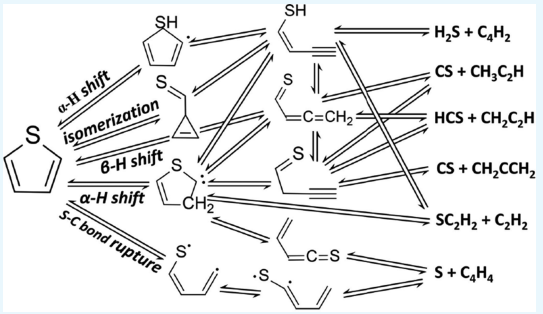

1. INTRODUCTION

Petroleum is the largest source of global energy consumption, supplying more than 33.1% of total world energy consumption.[1] Predicted by *BP p.l.c.*, petroleum will continue to take an important part in the global energy system for decades to come.[1]

Sulfur is an element commonly found in crude oil and petroleum products. In petroleum refining, sulfur is an undesirable impurity that could cause the deactivation of the catalysts and corrosion problems in pipelines and pumping and refining equipment.[2,3] Moreover, combustion of sulfur in fuels leads to the emission of sulfur oxides (SO_x), which are the important contributors to acid rain that can damage plants, crops, and structural surfaces.[4,5] In addition, the toxic SO_x released into air can interact with ozone, other gases, and particulates to form airborne sulfonated smog particles that are hazardous to human health.[6] Consequently, tighter regulations to minimize the negative effects have been legislated worldwide.[7−11]

Several processes have been recommended for the removal of sulfur from fuel.[12−18] The most common technique to remove sulfur from crude oil in the petroleum industry is hydrodesulfurization (HDS). However, HDS is less effective in treating thiophenes[19−21] that are present at significant levels in most petroleum,[22−26] especially alkyl dibenzothiophenes.[19] Studies have shown that thiophenes have high thermal stability at even high temperatures and pressures.[27,28] Hence, the knowledge on the pyrolysis mechanism of thiophenes is of significance in promoting desulfurization.

As the simplest thiophene sulfur, thiophene (C_4H_4S) is worthy of a detailed investigation as it could be a representative for all thiophenes. In 1959, Wynberg and Bantjes[29] studied thiophene cracking in a continuous flow reactor and identified dithiophenes, carbon disulfide, free carbon, hydrogen sulfide, and hydrocarbons in the pyrolysis products. Later, Cullis and Norris[30] performed thiophene pyrolysis under carbon formation conditions and commented that hydrogen sulfide was one of the major products. In 2002, Winkler et al.[31] studied thiophene pyrolysis using a quartz continuous flow reactor. In addition to methane, benzene, and hydrogen sulfide, a large number of secondary condensation products were identified as the pyrolysis products of thiophene. Memon et al.[32] performed thiophene thermolysis (1598−2022 K) in a shock tube. At all temperatures, acetylene was found to be the dominant product; ethene, ethanethiol, hydrogen sulfide, carbon disulfide, and several oligomers were also detected. Hore and Russell[33] investigated the laser

Received: May 12, 2021
Accepted: July 13, 2021
Published: July 28, 2021

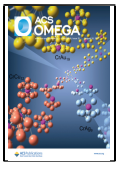

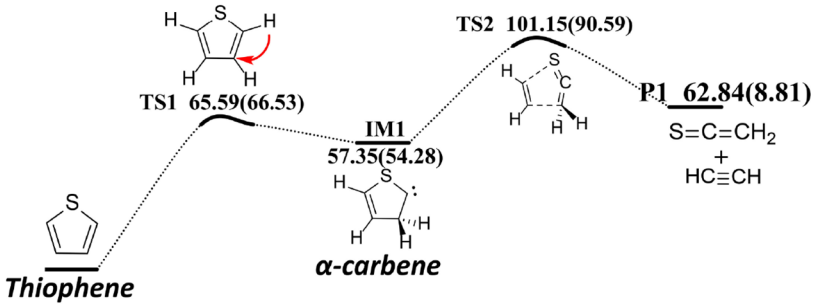

Figure 1. Potential energy surface of *Channel 1*. The values in parentheses are Gibbs energies at 1500 K, 1 atm (unit: kcal/mol).

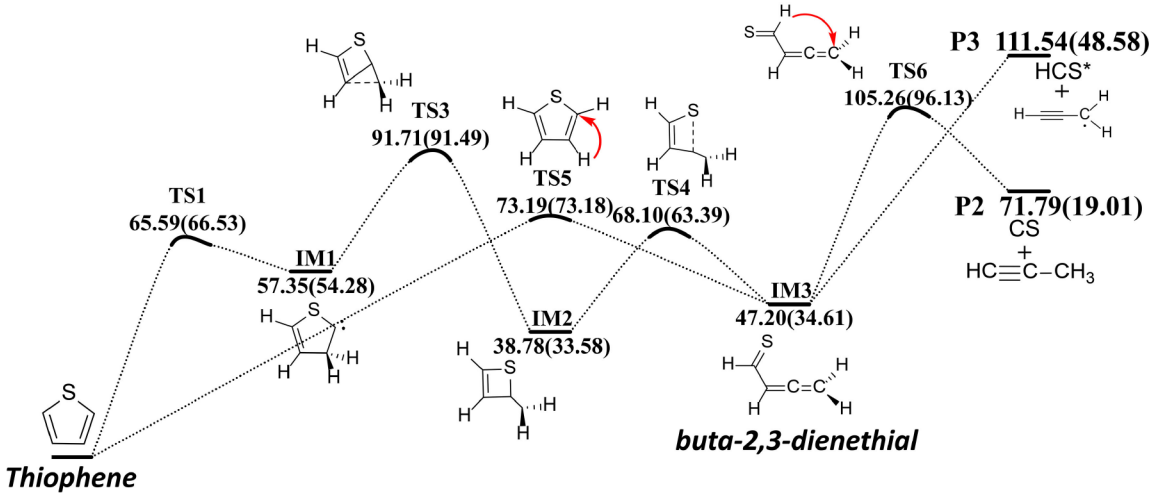

Figure 2. Potential energy surface of *Channel 2*. The values in parentheses are Gibbs energies at 1500 K, 1 atm (unit: kcal/mol).

pyrolysis of thiophene and declared that acetylene was the major gas-phase product. More recent contribution was made by Vasiliou et al.,[34] who carried out a thiophene decomposition experiment using a microtublar reactor and identified five groups of products. Quantum calculation methods[35−37] have also been applied to study the unimolecular pyrolysis mechanism of thiophene.

Most studies on thiophene pyrolysis have been focused on identifying decomposition products. As the secondary reactions between products cannot be excluded, the primary products inevitably change in different studies. By contrast, the pyrolysis rate of thiophene is less affected by the secondary reactions. So far, only two studies[34,53] involving the kinetics of thiophene pyrolysis have been reported. No kinetic model of thiophene unimolecular pyrolysis has been reported yet. Hence, the objective of this study is to investigate the unimolecular pyrolysis of thiophene and therefore develop a kinetic model. In this work, high-level ab initio methods were first used to investigate the pyrolysis reactions. Following this, rate coefficients of important elementary reactions were deduced using variational transition-state theory (VTST) at the CCSD(T)/CBS level. Based on the kinetic results, a kinetic model for the unimolecular pyrolysis of thiophene was developed.

2. RESULTS AND DISCUSSION

2.1. Major Mechanism. The major mechanism of thiophene unimolecular pyrolysis is concluded based on our preceding studies.[45−48] All possible initiations, including H shifts, ring bond ruptures, isomerization (non-H-migration), and C−H fission, have been considered in this work.

2.1.1. Channel 1—Decomposition via α-Carbene. Figure 1 presents the reaction details of this channel.

Thiophene converts to α-carbene via a 2,3-H shift and subsequently cracks to SC_2H_2 + C_2H_2 (thioketene + ethylene, P1) via concerted C_5-S_1 and C_3-C_4 cleavage. Song and Parish[37] reported that the potential energy of TS2 is 41.06 kcal/mol above α-carbene at the CBS-QB3 level. Our CCSD(T)/CBS calculation indicates that this value is 43.80 kcal/mol. This reaction channel could be represented by eqs 1 and 2

$$\text{thiophene} \rightarrow \text{IM1} \quad (1)$$

$$\text{IM2} \rightarrow \text{P1} \quad (2)$$

2.1.2. Channel 2—Decomposition via Buta-2,3-dienethial. The potential energy surface is presented in Figure 2.

In *Channel 2*, the ring-opening intermediate, IM3 (buta-2,3-dienethial), could be formed through two parallel pathways. One pathway starts with the isomerization of α-carbene to the four-ring intermediate IM2 and followed by ring opening at the S_1-C_3 bond. The transition state between IM1 and IM2 has an energy of 91.71 kcal/mol above thiophene. Additionally, thiophene could directly convert to IM3 via a 3,2-H shift, exhibiting a critical energy of 73.19 kcal/mol.

Decomposition of IM3 results in two groups of products, CS + CH_3C_2H (P2) and HCS* (radical) + C_3H_3* (P3). The former is generated via C_5-H migration to C_2. A barrier of 58.06 kcal/mol has been computed for this process. The later

https://doi.org/10.1021/acsomega.1c02155
ACS Omega 2021, 6, 20471−20482

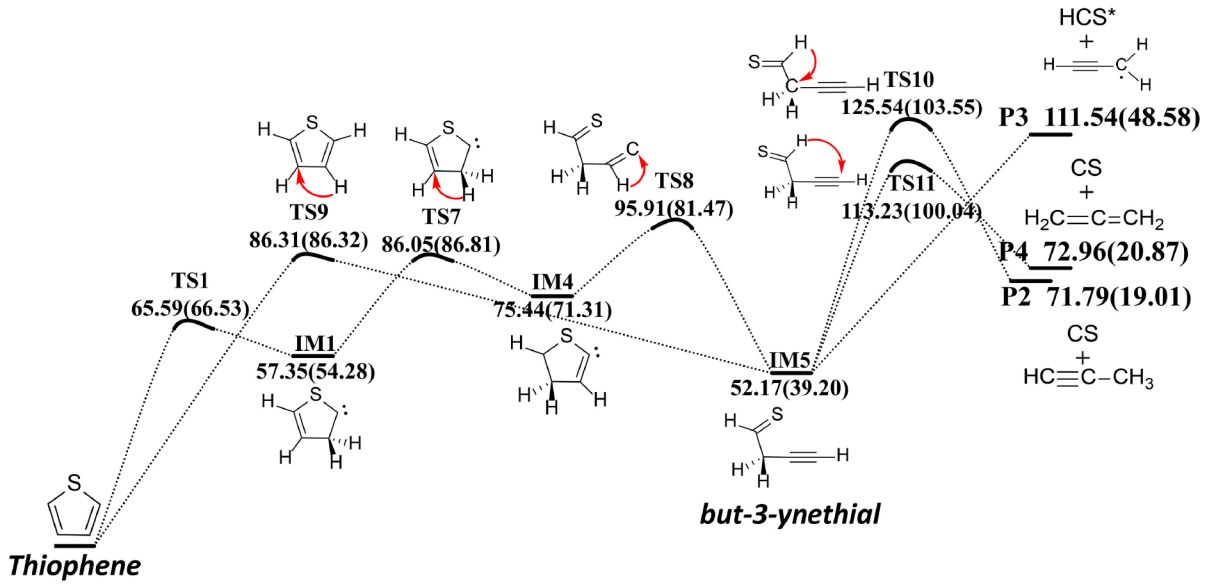

Figure 3. Potential energy surface of *Channel 3*. The values in parentheses are Gibbs energies at 1500 K, 1 atm (unit: kcal/mol).

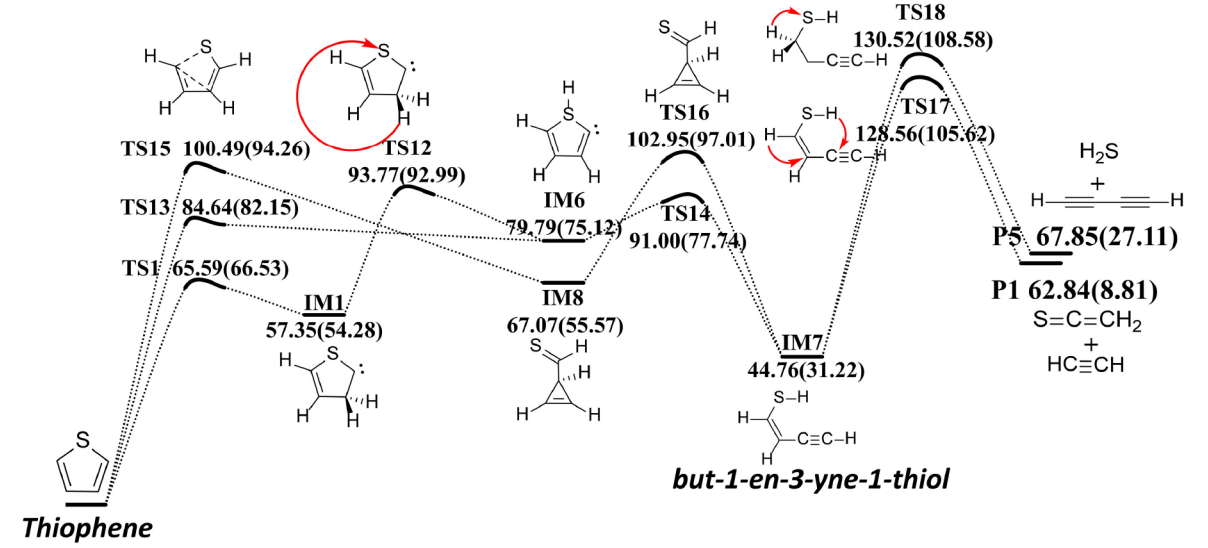

Figure 4. Potential energy surface of *Channel 4*. The values in parentheses are Gibbs energies at 1500 K, 1 atm. (unit: kcal/mol).

one is yielded through C_4-C_5 fission, which is endothermic by 64.34 kcal/mol at 0 K.

The elementary reactions in *Channel 2* can be illustrated as

thiophene → IM1 (1a)

IM1 → IM2 (3)

IM2 → IM3 (4)

thiophene → IM3 (5)

IM3 → P2 (6)

IM3 → P3 (7)

2.1.3. Channel 3—Decomposition via But-3-ynethial. Figure 3 depicts the energy profile of *Channel 3*.

Two independent pathways lead to the intermediate IM5, but-3-ynethial, which is the critical species for *Channel 3*. Intrinsic reaction coordinate (IRC) analysis verifies that thiophene could directly convert to IM5 through a 3,4-H shift. The barrier height was computed to be 86.31 kcal/mol at 0 K. Additionally, IM5 could be evolved from *α*-carbene via two H transfer steps, overcoming a barrier of 28.70 kcal/mol.

Decomposition of IM5 could result in three groups of products. Via C_5-H transfer to C_2 and C_4 sites, IM5 cracks to CS + CH_2CCH_2 (P4) and CS + CH_3C_2H (P2), respectively. The corresponding energy barriers are 61.06 and 73.37 kcal/mol. However, HCS* + C_3H_3* (P3) is yielded through C_5-C_4 bond cleavage, endothermic by 72.03 kcal/mol at 0 K.

The elementary reaction of *Channel 3* can be concluded as follows:

thiophene → IM1 (1b)

IM1 → IM5 (8)

thiophene → IM5 (9)

IM5 → P2 (10)

IM5 → P3 (11)

https://doi.org/10.1021/acsomega.1c02155
ACS Omega 2021, 6, 20471−20482

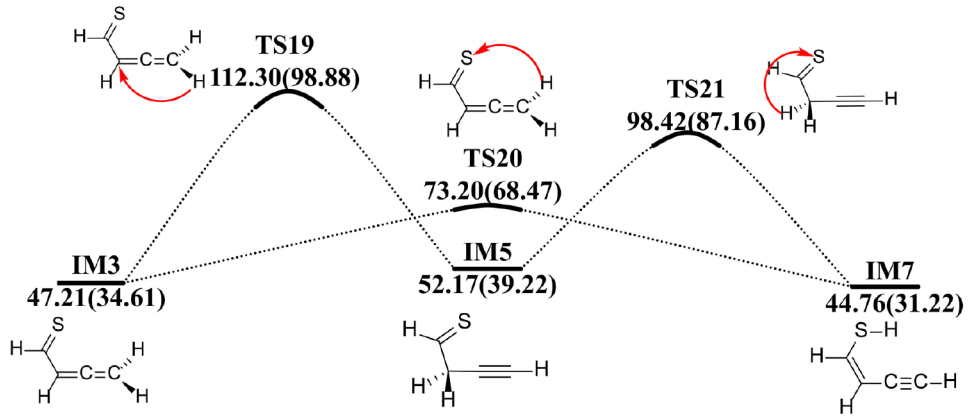

Figure 5. Conversion between IM3, IM5, and IM7. The values in parentheses are Gibbs energies at 1500 K, 1 atm (unit: kcal/mol).

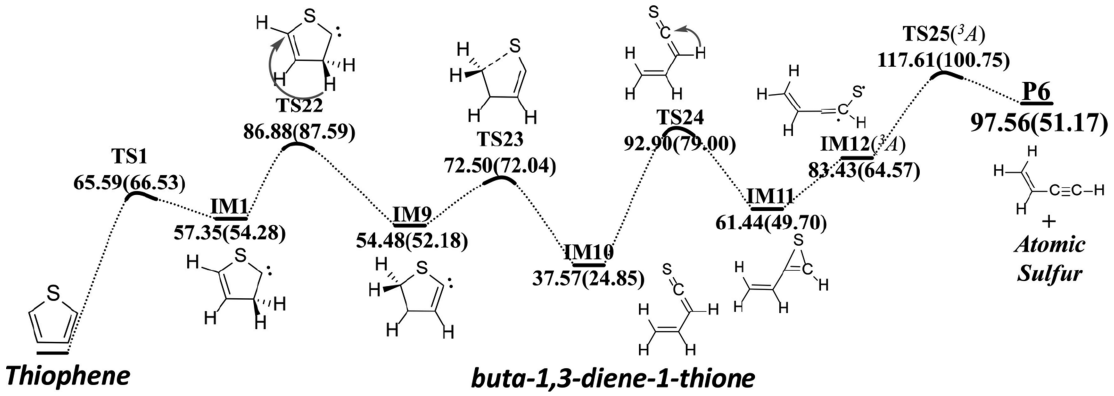

Figure 6. Potential energy surface of *Channel 5*. The values in parentheses are Gibbs energies at 1500 K, 1 atm (unit: kcal/mol).

IM5 → P4 (12)

2.1.4. Channel 4—Decomposition via But-3-yne-1-thiol. The potential energy surface is presented in Figure 4.

In *Channel 4*, IM7, but-1-en-3-yne-1-thiol is converted from thiophene through three independent pathways. The H shifts of thiophene from the C_2 (via C_3) to the S_1 site form carbene intermediate IM6, with a maximum barrier of 93.77 kcal/mol, whereas the 1-H shift of thiophene, directly producing IM6, has a computed barrier of 84.64 kcal/mol. IM6 could readily transform to IM7, exhibiting a barrier of 11.21 kcal/mol. Besides, thiophene could first isomerize to intermediate IM8 via TS15 and subsequently convert to IM7 through the migration of C_3−H to the S_1 site. CCSD(T)/CBS indicated that this pathway needs to overcome an energy barrier of 102.95 kcal/mol.

Decomposition of IM7 could proceed via two routes. SC_2H_2 + C_2H_2 (P1) is yielded from IM7 through S_1−H shifts to C_3 accompanied by C_5−H transfer to C_4. The transition state has been located at 83.80 kcal/mol above IM7, whereas H_2S + C_4H_2 (P5) is formed through C_4−H migration to S_1 via the C_5 site. The energy barrier is determined to be 85.76 kcal/mol.

The pathway of *Channel 4* can be represented by

thiophene → IM1 (1c)

IM1 → IM6 (13)

IM6 → IM7 (14)

thiophene → IM6 (15)

thiophene → IM7 (16)

IM7 → P1 (17)

IM7 → P5 (18)

It has been noticed that *Channel 2*, *Channel 3*, and *Channel 4* are connected by the H migration process, as shown in Figure 5.

It is indicated by the energy barrier and Gibbs energy that the processes of IM3−IM7 and IM5−IM7 are more important than IM3−IM5

IM3 → IM7 (19)

IM5 → IM7 (20)

2.1.5. Channel 5—Decomposition via Buta-1,3-diene-1-thione. Details of this channel are illustrated in Figure 6.

Starting with the 2,3-H shift, thiophene first converts to *α*-carbene and thus undergoes a C_3−H shift to C_5, forming another carbene intermediate IM9. The overall barrier height of this process is 86.88 kcal/mol, located at the IM1 → IM9 step. The subsequent ring opening of IM9 gives IM10, exhibiting a barrier of 18.02 kcal/mol. IM10 undergoes C_3−H migration to C_2, giving the C−S−C three-ring intermediate IM11. The following cleavage of the S_1−C_3 bond leads to the triplet intermediate IM12(^3A). Atomic sulfur (P6) is produced through the elimination of sulfur via the transition state TS25(^3A), of which the energy is 56.17 kcal/mol above IM11.

The important reactions in *Channel 5* can be concluded as

thiophene → IM1 (1d)

IM1 → IM10 (21)

https://doi.org/10.1021/acsomega.1c02155
ACS Omega 2021, 6, 20471−20482

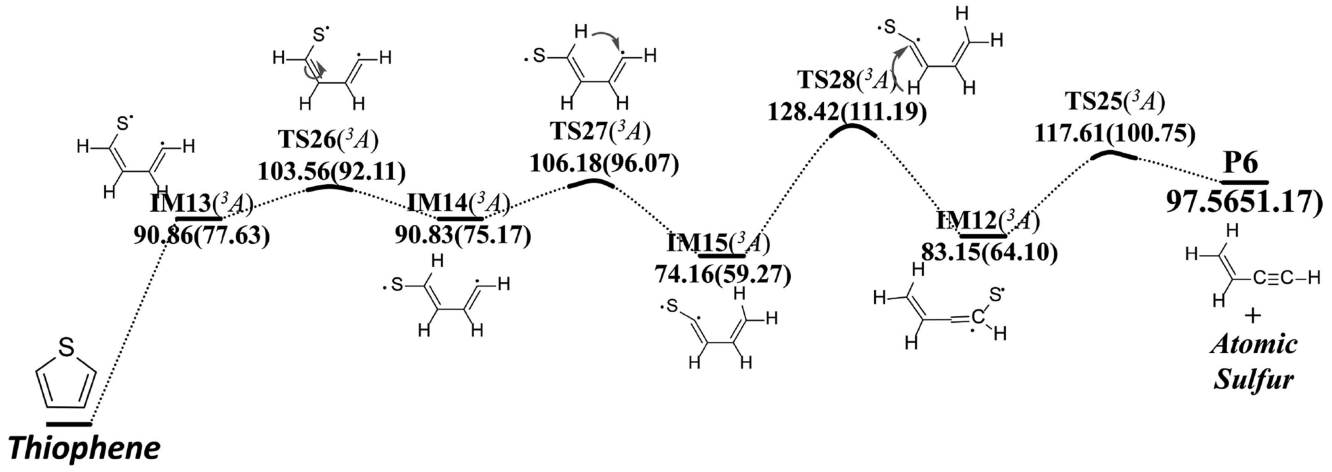

Figure 7. Potential energy surface of *Channel 6*. The values in parentheses are Gibbs energies at 1500 K, 1 atm (unit: kcal/mol).

IM10 → P6 (22)

2.1.6. Channel 6—Decomposition via Bond Rupture. Ring bond rupture has been proposed as the initiation of thiophene pyrolysis in preceding. However, the relative importance of this channel has not been reported yet. In this work, this pathway has also been investigated. The potential energy surface is presented in Figure 7.

The cleavage of the S−C bond, forming triplet intermediate IM13(^3A), endothermic by 90.86 kcal/mol at 0 K. IM15(^3A) is converted via C_5-C_4 bond rotation and subsequent C_5-H migration. Decomposition of IM15(^3A) proceeds via two steps. The first step is the H transfer from C_4 to C_5, giving the triplet intermediate of IM12(^3A). The following step is the elimination of sulfur via transition state TS23(^3A). Judging from the Gibbs free energy, the process of IM15(^3A) → IM12(^3A) is supposed to be the rate-limiting step of *Channel 6*. The overall reaction of this channel is given by eq 23

thiophene → P6 (23)

2.1.7. Channel 7—Decomposition via Simple Ring-H Fission. The fission of the C−H bond could either be a possible initiation for thiophene pyrolysis. In previous study, we have compared the C−H bonds of thiophene, furan, and benzene. It is indicated that the C−H bond of thiophene is stronger than that of benzene, however energetically similar to furan. We assumed that the recombination rate constant of H + 2-/3-thienyl → thiophene is identical to that of H + 2-/3-furyl → furan and thus estimated the dissociation rate constant through the equilibrium constant and microscopic reversibility

H* + 2-thienyl* → thiophene (24)

H* + 3-thienyl* → thiophene (25)

To check the reliability of the CCSD(T)/CBS calculation, we have computed (including optimization) all stationary points at M062x/def2-QZVP, CBS-QB3, G4, and W1BD levels. Table 1 presents the relative energies of IMs and TSs at different levels.

All of these calculation methods give comparable results. The mean absolute energy deviation between CCSD(T)/CBS and W1BD is only 0.64 kcal/mol. This comparison led us to conclude that our CCSD(T)/CBS calculation is reliable in studying the kinetic behavior of thiophene.

2.2. Thermodynamic. To ensure the accuracy of thermodynamic calculations, the standard enthalpy change, $\Delta_f H^\Theta$ at 298 K, of the involved pyrolysis reaction has been calculated at various levels and compared to available experimental values in Table 2. Besides, we have contrasted the calculated thermodynamic properties (S^Θ and C_p at 298 K) with literature data for some species.

As can be seen in Table 2, the $\Delta_f H^\Theta$ values at 298 K of thiophene pyrolysis derived from different methods are in accordance with the experimental values within chemical accuracy. The calculated C_2-H and C_3-H bond strengths are also identical to our CCSD(T)/CBS results. The comparison of S^Θ and C_p at 298 K (in Table S4) shows that our calculations are in good agreement with the literature values within the uncertainties. These discussions further convinced us that CCSD(T)/CBS is accurate in describing the kinetics of thiophene pyrolysis.

To deduce the thermodynamic product, the Gibbs free energy change ΔG of thiophene pyrolysis has been computed. For comparison purposes, the ΔG was either obtained using M062x/def2-QZVP, CBS-QB3, G4, and W1BD methods. Results are shown in Figure 8.

From Figure 8, it can be seen that the results given by these methods are approximate. Compared with other methods, the G4 method may underestimate the Gibbs free energy of products for most cases. However, the results of CBS-QB3 are more close to those of CCSD(T)/CBS and W1BD that are theoretically more accurate.

The decomposition of thiophene to SC_2H_2 + C_2H_2 (P1) is thermodynamically preferred to other products at all temperatures. P1 is the most stable product that could be directly produced from thiophene. The spontaneous temperature (ΔG = 0) is around 1695 K. Thermolysis of thiophene to CS + CH_3C_2H (P2) and CS + CH_2CCH_2 (P3) has a similar thermodynamic character. The spontaneous temperatures for P2 and P4 are around 1930 and 1980 K, respectively. The importance of P2 and P4 is only secondary to P1.

By contrast, the formation of HCS* + C_3H_3* (P3) and H_2S + C_4H_2 (P5) is highly endergonic. The favored temperatures for P3 and P5 are above 2425 and 2300 K at the CCSD(T)/CBS level, respectively. The group of atomic sulfur + C_4H_4 is the most endothermic product among these products. The spontaneous temperature, i.e., 2825 K, indicates that atomic sulfur is less likely to be a major product of thiophene.

https://doi.org/10.1021/acsomega.1c02155
ACS Omega 2021, 6, 20471−20482

Table 1. Relative Energy (0 K) of All Intermediates, Transition States, and Products at M062x/def2-QZVP, CBS-QB3, G4, W1BD, and CCSD(T)/CBS Levels[a]

species	M062x/def2-QZVP	CBS-QB3	G4	W1BD	CCSD(T)/CBS
IM1	58.85	58.31	57.31	57.73	57.35
IM2	39.67	39.20	38.62	39.16	38.78
IM3	46.39	46.91	46.48	47.90	47.21
IM4	77.27	76.21	74.97	75.64	75.44
IM5	52.70	52.28	51.61	52.87	52.17
IM6	81.34	81.11	80.09	80.00	79.79
IM7	43.48	45.63	45.10	45.35	44.76
IM9	56.18	56.21	54.55	54.91	54.48
IM10	36.22	36.84	36.19	38.00	37.57
IM11	59.00	61.59	60.84	61.82	61.44
IM12	79.83	81.88	82.78	83.64	83.43
IM13	86.62	88.41	90.92	90.50	90.86
IM14	86.86	89.23	90.53	90.91	90.83
IM15	72.56	72.96	73.64	74.52	74.36
TS1	65.24	66.83	66.06	66.05	65.59
TS2	102.69	99.40	99.74	101.87	101.15
TS3	92.52	91.49	91.21	92.42	91.71
TS4	69.07	67.17	67.14	68.99	68.10
TS5	73.08	74.58	73.88	73.78	73.19
TS6	110.82	105.50	103.94	106.79	105.26
TS7	86.20	85.91	85.98	86.34	86.05
TS8	95.65	96.89	95.58	97.14	95.91
TS9	86.83	86.73	86.36	86.68	86.31
TS10	130.17	124.82	124.03	126.48	125.54
TS11	117.69	112.43	112.10	114.50	113.23
TS12	94.94	94.41	93.83	93.86	93.77
TS13	85.47	85.82	85.25	84.93	84.64
TS14	91.86	93.86	92.85	92.14	91.00
TS15	91.86	99.76	99.23	101.96	100.49
TS16	101.61	103.83	103.55	104.08	102.95
TS17	128.01	129.45	128.34	129.77	128.56
TS18	131.65	129.80	128.99	131.62	130.52
TS19	115.64	111.22	110.23	113.32	112.30
TS20	75.02	73.66	73.03	74.12	73.20
TS21	100.63	97.40	96.18	99.99	98.42
TS22	86.75	87.78	87.00	87.28	86.88
TS23	75.59	70.69	71.22	73.00	72.50
TS24	90.64	92.99	92.23	93.86	92.90
TS25[b]	115.74				117.61
TS26	101.55	103.69	102.39	104.28	103.56
TS27	104.10	103.52	106.32	105.83	106.18
TS28	123.96	127.30	127.43	128.73	128.42
P1	62.12	62.44	61.31	63.29	62.84
P2	74.31	71.93	70.49	72.79	71.79
P3	111.38	110.14	109.32	111.43	111.54
P4	74.44	72.90	72.65	73.88	72.96
P5	69.11	69.40	68.97	68.60	67.85
P6	98.37	99.29	97.67	98.47	97.56

[a]Unit: kcal/mol. [b]Transition state TS25 could be located only at the M062x/def2-QZVP level. The geometry optimized at the M062x/def2-QZVP level was further used to obtain CCSD(T)/CBS energy of TS25.

Based on the discussion above, it is concluded that SC_2H_2 + C_2H_2 (P1), CS + CH_3C_2H (P2), and CS + CH_2CCH_2 (P4) are the principal products of thiophene, whereas the appearance of HCS* + C_3H_3* (P3), H_2S + C_4H_2 (P5), and atomic sulfur + C_4H_4 (P6) needs higher temperatures. All of these of products, except P4, have been detected by Vasiliou et al.[34] in the microtubular reactor pyrolysis experiment. The absence of CH_2CCH_2 may be caused by the kinetic competition between P2 and P4. On the contrary, the detection of HCS*, as well as SC_2H_2, at the beginning temperature of pyrolysis (1300 K) indicates that HCS* is likely a kinetic product.

2.3. Kinetics and Modeling. The high-pressure limit rate constant, k, of elementary reactions was calculated using the VTST-CCSD(T)/CBS method and subsequently fitted to the modified three-parameter Arrhenius expression $k = A \times T^n \times \exp[-E_a/(RT)]$. For the four barrierless reactions, namely, IM3 → P3 (7), IM5 → P3 (11), TRE → H + 2-thienyl (24), and TRE → H + 3-thienyl (25), we estimated the rate constants by analogy to the similar reaction in furan pyrolysis. Particularly, the rate constants of IM3 → P3 (7) and IM5 → P3 (11) are estimated from the reaction of buta-2,3-dienal → formyl radical + propargyl radical.[51] The C_2−H and C_3−H loss rates of thiophene were estimated by analogy to that of furan.[52] Rate coefficients of the elementary reactions in the kinetic model are presented in Table 3.

To verify the model, the unimolecular pyrolysis rate of thiophene in the 1300−1800 K range has been computed. A small residence time of 100 μs was used in the modeling to avoid the effect of secondary reactions. The results are demonstrated in Figure 9.

From Figure 9, it can be seen that all of the Arrhenius plots are located on a straight line. Least-squares regression analysis implies that the pyrolysis rate of thiophene could be given by eq 26

$$k = 1.21 \times 10^{13} \times \exp[(78.96\ \text{kcal/mol})/(RT)] \quad (26)$$

The square of the correlation coefficient, r^2 (i.e., 0.9973), indicates that our results in 1300−1700 K are in good agreement with the results of the higher-temperature range and lower-temperature range. However, we also noticed that the decomposition of thiophene to C_2H_2 + SC_2H_2 is proceeding at a rather high rate above 2000 K. At such a high temperature, the secondary reactions may play a more significant role in thiophene pyrolysis. Hence, the suggested temperature range for this model is 1300−1700 K.

We further applied this model to study thiophene pyrolysis. The unimolecular pyrolysis of thiophene was modeled at 1300, 1400, 1500, and 1600 K. The product distribution of thiophene unimolecular pyrolysis at different temperatures is shown in Figure 10.

As can be seen from Figure 10, the amount of SC_2H_2 + C_2H_2 (P1) in the product is significant at all modeling temperatures. Both the kinetics and thermodynamics indicate that SC_2H_2 + C_2H_2 is the principal pyrolysis product of thiophene. The reaction of α-carbene → P1 is concluded to be the principal formation route for SC_2H_2 + C_2H_2. In previous study, the feasibility of SC_2H_2 + C_2H_2 formation during thiophene pyrolysis has been discussed. Song and Parish[37] proposed SC_2H_2 + C_2H_2 as a major product of thiophene based on their CBS-QB3 calculation. Vasiliou et al.[34] detected SC_2H_2 + C_2H_2 at the beginning pyrolysis temperature (i.e., 1300 K) in the microtubular reactor pyrolysis experiment. Memon et al.[32] identified C_2H_2 as the principal hydrocarbon product at 1559−2022 K. However, no SC_2H_2 was found in their experiment. It seems that SC_2H_2 is first produced accompanied by C_2H_2 and subsequently consumed rapidly. This could be partly explained by the reaction of eq 27

https://doi.org/10.1021/acsomega.1c02155
ACS Omega 2021, 6, 20471−20482

Table 2. Standard Enthalpy Change ($\Delta_f H^{\Theta}$, 298 K) of the Thiophene Pyrolysis Reaction[a]

	M062x/def2-QZVP	CBS-QB3	G4	W1BD	CCSD(T)/CBS	reference
thiophene → P1	74.94	75.29	74.22	76.13	75.69	
thiophene → P2	87.33	84.95	83.56	85.80	84.81	83.01[b]
thiophene → P3	126.42	125.22	124.51	126.51	126.62	123.75[b]
thiophene → P4	87.36	85.75	84.44	86.74	85.83	84.45[b]
thiophene → P5	77.85	78.55	78.21	78.01	77.27	77.35[b]
thiophene → P6	109.39	110.28	108.69	109.47	108.56	107.28[b]
thiophene → H + 2-thienyl	116.44	118.40	116.99	118.44	119.04	119.2[c], 118.39[d]
thiophene → H + 3-thienyl	114.06	115.95	114.65	116.05	116.65	117.0[c], 115.93[d]

[a]Unit: kcal/mol. [b]Experimental results, calculated based on the thermodynamic data of Goos et al.[49] [c]By Barckholtz et al.[50] at the CBS-Q level. [d]By Song and Parish[37] at the CBS-QB3 level.

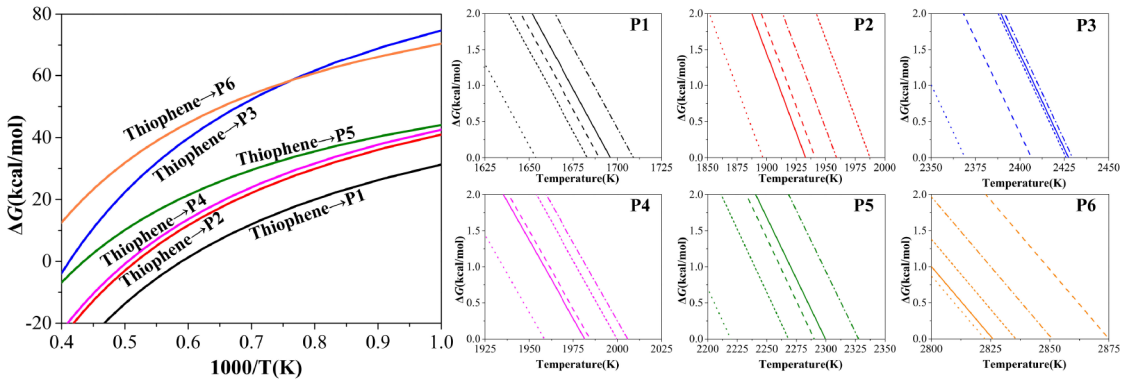

Figure 8. Gibbs free energy change ΔG of thiophene pyrolysis. Solid line, CCSD(T)/CBS; short dash line, M062x/def2-QZVP; dash line, CBS-QB3; dot line, G4; dash dot line, W1BD.

$$CS + SC_2H_2 \rightarrow CS_2 + C_2H_2 \quad (27)$$

The ΔG of eq 26 is barely effected by temperature, −30.64 kcal/mol at 298 K and −24.75 kcal/mol at 1500 K. CS_2 could be converted indirectly in thiophene pyrolysis by consuming CS and SC_2H_2. This is in accordance with the experimental result that CS_2 is one of the major sulfur-containing compound of thiophene pyrolysis.[34] Besides, the decomposition of SC_2H_2 through eq 28 is favored at higher temperatures

$$2SC_2H_2 \rightarrow S_2 + 2C_2H_2 \quad (28)$$

The ΔG_{R27} is −0.85 kcal/mol at 1500 K. We concluded that $SC_2H_2 + C_2H_2$ is the major primary product of thiophene pyrolysis. Its behavior in the products is important in understanding the mechanism of final stable product formation.

In addition to $SC_2H_2 + C_2H_2$, HCS* + C_3H_3* (P3) is also yielded in an significant amount. HCS* may be of similar importance to SC_2H_2 in thiophene pyrolysis. Vasiliou et al.[34] confirmed that HCS*, as well as SC_2H_2, is formed at the beginning pyrolysis temperature of 1300 K. However, in the shock tube experiment of Memon et al.,[32] HCS* was traceless over the temperature of 1559−2022 K. This may be accounted for by the reactions of eqs 29 and 30

$$2HCS^* \rightarrow H_2 + 2CS \quad (29)$$

$$HCS^* + H \rightarrow H_2 + CS \quad (30)$$

The ΔG_{R28} and ΔG_{R29} are −32.42 and −48.79 kcal/mol at 1500 K (−7.17 and −52.18 kcal/mol at 298 K), respectively. As the rate coefficient for HCS* formation is estimated from a similar reaction in this modeling, certain uncertainties of the HCS* content may exist. Combining previous experimental results and our kinetic modeling results, HCS* + C_3H_3* is expected to be a significant product of thiophene unimolecular thiophene pyrolysis.

CS is another sulfur-containing product of thiophene pyrolysis. The corresponding hydrocarbon products are CH_3C_2H and CH_2CCH_2. In modeling, CH_2CCH_2 is present at a much lower level compared with CH_3C_2H, which is consistent with the results of the pyrolysis experiment.[36] The modeling results also manifest that the formation of CS is promoted at higher temperatures. The mole ratio of CS/SC_2H_2 in the product is merely 1:10 at 1300 K, whereas this value have exceeded to 1:3 at 1600 K. Production of CS has been confirmed in the microtublar reactor experiment at 1400 K and above.[34] However, none CS was detected in the pyrolysis experiment of the shock tube.[32] Based on the discussion above, we suppose CS as an important direct product of thiophene pyrolysis.

The amount of atomic sulfur + C_4H_4 in the product is negligible for its high formation barrier. Vasiliou et al.[34] detected atomic sulfur during thiophene pyrolysis at 1500 K. However, the source of atomic sulfur from other sulfur-containing products cannot be excluded. In the shock tube experiment by Memon et al.,[32] no atomic sulfur was detected over the temperature range of 1598−2022 K. Atomic sulfur is less likely to be important. However, the atomic sulfur evolved from other sulfur-containing products could promote the variation of sulfur-containing hydrocarbon compounds.

Similar to atomic sulfur, the amount of H_2S is also ignorable even at highly elevated temperatures. Our results are basically consistent with the experimental result that H_2S was detected only at a higher temperature (1500 K) than SC_2H_2, HCS*, and CS.[34] Surprisingly, Memon et al.[32] found that H_2S is present at a significant level in products, which is much higher than its

https://doi.org/10.1021/acsomega.1c02155
ACS Omega 2021, 6, 20471−20482

Table 3. Rate Coefficients $k = A \times T^n \times \exp[-E_a/(RT)]$ of the Elementary Reactions Involved in the Unimolecular Decomposition of Thiophene for 1300−1700 K[a]

		$k(T) = A \times T^n \times \exp[-E_a/(RT)]$		
no.	reaction	A	T	E_a
R1	TRE → IM1	4.49×10^{13}	0.16	67.08
	reverse	7.39×10^{12}	0.13	8.73
R2	IM1 → P1	1.23×10^{16}	−0.31	47.71
	reverse	4.44×10^{3}	2.23	26.20
R3	IM2 → IM1	9.63×10^{12}	0.05	53.50
	reverse	3.27×10^{13}	0.00	35.24
R4	IM3 → IM2	7.43×10^{12}	0.04	21.30
	reverse	5.51×10^{13}	0.05	30.42
R5	TRE → IM3	6.53×10^{13}	0.14	74.92
	reverse	2.38×10^{11}	0.14	25.80
R6	IM3 → P2	1.20×10^{13}	0.21	62.89
	reverse	8.00×10^{2}	2.61	19.80
R7[b]	IM3═P3	4.00×10^{24}	−3.00	70.26
R8	IM1 → IM5	5.17×10^{17}	−0.88	40.92
	reverse	8.19×10^{15}	−0.82	44.90
R9	TRE → IM5	2.28×10^{13}	0.29	87.65
	reverse	1.82×10^{11}	0.19	34.00
R10	IM5 → P2	1.65×10^{15}	0.10	76.38
	reverse	5.37×10^{4}	2.60	42.90
R11[b]	IM5═P3	3.29×10^{24}	−3.00	70.47
R12	IM5 → P4	1.08×10^{13}	0.23	62.11
	reverse	0.21	3.13	−15.40
R13	IM6 → IM1	9.75×10^{11}	0.14	48.36
	reverse	7.63×10^{13}	0.12	37.78
R14	IM6 → IM7	5.92×10^{14}	0.09	13.39
	reverse	2.17×10^{13}	0.09	47.48
R15	TRE → IM6	1.50×10^{14}	0.19	86.91
	reverse	1.82×10^{13}	0.10	5.48
R16	TRE → IM7	2.60×10^{13}	0.56	104.65
	reverse	4.22×10^{12}	0.14	59.10
R17	IM7 → P1	1.74×10^{14}	0.02	84.24
	reverse	2.68×10^{7}	1.65	56.90
R18	IM7 → P5	1.02×10^{15}	0.22	88.71
	reverse	2.68×10^{5}	3.07	54.10
R19	IM7 → IM3	1.18×10^{12}	0.13	28.70
	reverse	1.50×10^{12}	0.18	27.18
R20	IM7 → IM5	6.05×10^{13}	−0.07	55.10
	reverse	7.30×10^{13}	−0.03	48.49
R21	IM1 → IM10	1.95×10^{13}	0.12	30.29
	reverse	3.88×10^{11}	0.17	49.40
R22	IM10═P6	1.55×10^{14}	−0.37	71.35
R23	TRE → P6	1.98×10^{12}	1.39	126.30
	reverse	2.70×10^{8}	1.74	22.10
R24[c]	TRE → H + 2-thienyl	1.55×10^{13}	0.52	112.61
R25[c]	TRE → H + 3-thienyl	1.18×10^{13}	0.55	110.14

[a]Units: s, cm, mol, and kcal. [b]Estimated from a similar reaction of furan.[51] [c]Estimated from a similar reaction of furan.[52]

corresponding hydrocarbon compound C_4H_2. As the atomic hydrogen that is produced directly from ring-H fission is negligible, the explanation that H_2S is produced through secondary reactions (eqs 31−37) is preferred by this work. The ΔG values of R30−R36 have been calculated at the CCSD(T)/CBS level and are presented in Table 4.

In studying furan thermal decomposition, Sendt et al.[51] proposed the mechanism of eq 31 as an important path for atomic hydrogen. Considering that the pyrolysis temperature

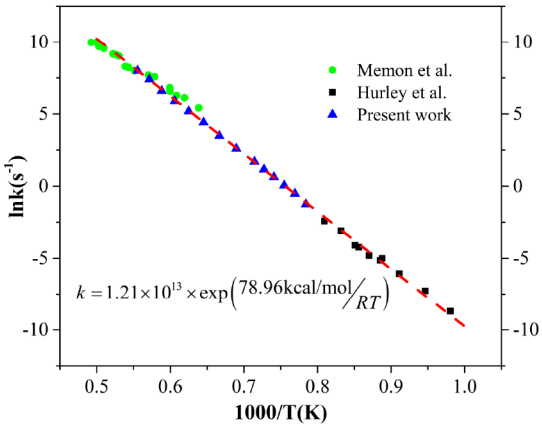

Figure 9. Comparison of the Arrhenius plot of thiophene decomposition. The data of Memon et al. and Hurley et al. were taken from refs 32 and 53, respectively.

of thiophene is much higher than that of furan, the H loss reaction of CH_3C_2H is supposed to be an important source of atomic hydrogen in thiophene pyrolysis and further leads to the formation of H_2S.

Based on the discussion above, we conclude that the unimolecular pyrolysis of thiophene mainly starts with ring-H migration, namely, C_2−H migrations and C_3−H migrations. By contrast, the cleavage of the C−S bond has limited contribution to the overall pyrolysis rate. The major mechanism of thiophene unimolecular pyrolysis is the conversion and decomposition of α-carbene (IM1), buta-2,3-dienethial (IM3), and but-3-ynethial (IM5). SC_2H_2 + C_2H_2 (P1), CS + CH_3C_2H (P2), and HCS* + C_3H_3* (P3) are concluded to be the principal direct products. However, these direct products could be further converted to more stable sulfur species through the secondary relations.

Compared with the unimolecular pyrolysis mechanism, the secondary reactions between products may be more complicated. The high temperature promotes the condensation and decomposition of hydrocarbon products, leading to various hydrocarbon species and sulfur-containing species. In this work, we mainly concentrated on the unimolecular thermolysis mechanism of thiophene. However, these secondary reactions have an important significance in understanding the complete mechanism of thiophene pyrolysis. In the following study, we will focus on the secondary reactions to develop a more comprehensive kinetic model.

3. CONCLUSIONS

In this work, high-level ab initio methods were adopted to investigate the unimolecular pyrolysis of thiophene. All possible initiation reactions, including ring-H migration, C−S bond fission, non-H-migration isomerization, and simple ring-H fission, have been considered. The mechanisms are shown in Figure 11.

Rate coefficients of the elementary reactions have been computed using variational transition state theory at the CCSD(T)/CBS level to develop a kinetic model for thiophene unimolecular pyrolysis. The calculated pyrolysis rate of thiophene is in good agreement with preceding experimental results, which could be given by eq 38

$$k = 1.21 \times 10^{13} \times \exp[(78.96\ \text{kcal/mol})/RT] \quad (38)$$

https://doi.org/10.1021/acsomega.1c02155
ACS Omega 2021, 6, 20471−20482

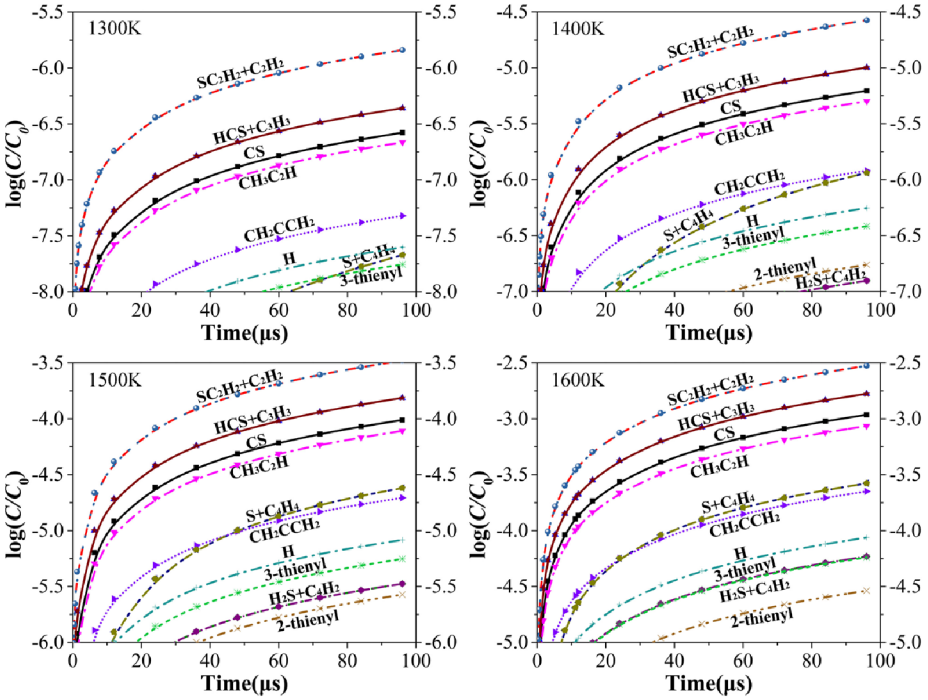

Figure 10. Product distribution of thiophene unimolecular pyrolysis at different temperatures. C_0 is the initial concentration of thiophene. Modeling conditions: 3 atm, thiophene 0.5%, Ar 99.5%.

Table 4. ΔG of the Reactions Related to H_2S Formation[a]

reaction	$\Delta G(T)$
$CH_3C_2H \rightarrow C_3H_3^* + H^*$ (31)	$-0.0323 \times T + 93.26$
$CH_2CCH_2 \rightarrow C_3H_3^* + H^*$ (32)	$-0.0328 \times T + 92.33$
$HCS^* \rightarrow CS + H$ (33)	$-0.0238 \times T + 52.10$
$2H^* + SC_2H_2 \rightarrow H_2S + C_2H_2$ (34)	$0.0213 \times T - 103.95$
$2H^* + S \rightarrow H_2S$ (35)	$0.0485 \times T - 178.01$
$2H^* + CS_2 \rightarrow CS + H_2S$ (36)	$0.0164 \times T - 71.43$
$4H^* + S_2 \rightarrow 2H_2S$ (37)	$0.0845 \times T - 292.67$

[a]Unit: kcal/mol, K.

Further applying this kinetic modeling in studying the pyrolysis product distribution, we found that the unimolecular pyrolysis of thiophene is mainly initiated by the ring-H migrations, whereas the C−S bond rupture and other initial steps have limited contribution to the overall pyrolysis rate. $SC_2H_2 + C_2H_2$ is found to be the major pyrolysis product at all temperatures. Significant amounts of HCS radical and CS are yielded. By contrast, the atomic sulfur and H_2S are present in negligible levels and likely to be produced through secondary reactions. The major principal products could be converted to other forms via secondary reactions.

4. COMPUTATIONAL DETAILS

4.1. Potential Energy Surface. All calculations were performed using the *Gaussian 09* package.[38] The harmonic vibrational frequencies of stationary points were computed to verify the nature of intermediates and transition states. IRC calculations[39] were also carried out to validate the connection between the transition state and designed reactant/product.

To improve the accuracy of relative energy, the CCSD(T) single point energy was calculated using cc-pVTZ and cc-pVQZ basis sets in the well-optimized geometry at the B3LYP/cc-pVTZ level. The spin eigenvalue of T1 diagnostic for the Hartree−Fock wave function[40] has been checked to ensure the reliability of the CCSD(T) calculation. The zero-point vibrational energy (ZPE) and thermodynamic correction energy were obtained from the result of the B3LYP/cc-pVTZ frequency using software *Shermo* 2.0.8.[41] To accurately determine the Gibbs free energy, the quasi-RRHO method proposed by Grimme et al.[42] has been adopted to treat the low frequencies of IMs and TSs. All energies reported in the figure of potential energy surface are CCSD(T)/CBS energies including the ZPE energy.

4.2. CBS Extrapolation. To obtain the CCSD(T)/CBS energy, the extrapolation method proposed by Helgaker et al.[43] has been employed. The CCSD(T)/CBS energy $E_{\mathrm{CCSD(T)}}^{(\infty)}$ could be expressed as the sum of the Hartree−Fock CBS energy $E_{\mathrm{HF}}^{(\infty)}$ and the correlation CBS energy $E_{\mathrm{corr}}^{(\infty)}$, as illustrated by eq 39

$$E_{\mathrm{CCSD(T)}}^{(\infty)} = E_{\mathrm{HF}}^{(\infty)} + E_{\mathrm{corr}}^{(\infty)} \quad (39)$$

For the reason that the Hartree−Fock energy $E_{\mathrm{HF}}^{(\infty)}$ and the correlation energy $E_{\mathrm{corr}}^{(\infty)}$ have apparently different converging characters, extrapolation of the Hartree−Fock energy and the correlation energy was carried out independently. The extrapolation of Hartree−Fock energy $E_{\mathrm{HF}}^{(\infty)}$ can be given by eq 40

$$E_{\mathrm{HF}}^{(X)} = E_{\mathrm{HF}}^{(\infty)} + A \cdot \exp(-\alpha \cdot X^{0.5}) \quad (40)$$

where X denotes the cardinality of the basis set and A is the constant needed to be parameterized during extrapolation. The recommended α is 5.46 for TZ/QZ extrapolations.[44] Equation 41 presents the extrapolation of the correlation energy $E_{\mathrm{corr}}^{(\infty)}$.

https://doi.org/10.1021/acsomega.1c02155
ACS Omega 2021, 6, 20471−20482

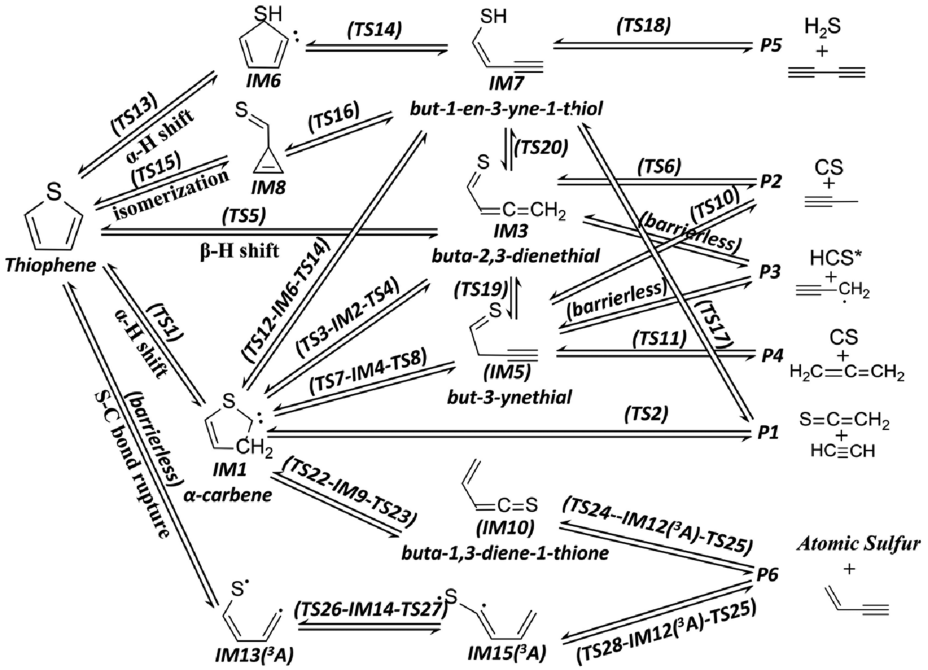

Figure 11. Sketch of the mechanism of thiophene unimolecular pyrolysis.

$$E_{corr}^{(\infty)} = \frac{X^{\beta}E_{corr}^{(X)} - Y^{\beta}E_{corr}^{(Y)}}{X^{\beta} - Y^{\beta}} \quad (41)$$

where X and Y are the cardinal numbers. The proposed value of β is 3 for TZ/QZ extrapolation.

4.3. Rate Coefficient Calculation. Rate coefficients of elementary reactions were calculated using VTST at the CCSD(T)/CBS level. The VTST rate constant k_{VTST} is given by eq 42

$$k_{VTST} = \sigma\frac{k_B T}{h}\frac{Q_{TS}}{Na\prod Q_{reac}}\exp\left(-\frac{\Delta E_0}{k_B T}\right) \quad (42)$$

where σ is the symmetry factor of reaction pathway. k_B and h are Boltzmann's constant and Planck's constant, respectively. Na is the Avogadro number. ΔE_0 is the maximum energy barrier along IRC excluding ZPE. Q_{TS} and Q_{reac} denote the total partition functions of the transition state and reactant with the translational partition functions expressed in per unit volume, respectively. In this work, the thermodynamic equivalent of eq 43 was employed

$$k_{VTST} = \sigma\frac{k_B T}{h}\left(\frac{RT}{P}\right)^{n-1}\exp\left(-\frac{\Delta G_{max}}{k_B T}\right) \quad (43)$$

where R is the gas constant and ΔG_{max} is the maximum Gibbs free energy barrier along the IRC path at the CCSD(T)/CBS level. Detailed procedure of the VTST-CCSD(T)/CBS calculation can be found in our previous work.[45]

■ ASSOCIATED CONTENT

Supporting Information

The Supporting Information is available free of charge at https://pubs.acs.org/doi/10.1021/acsomega.1c02155.

Geometries in the xyz format; only imaginary frequency of transition states; Gibbs free energies of all transition states and intermediates at B3LYP/cc-pVTZ, M062x/def2-QZVP, CBS-QB3, G4, W1BD, and CCSD(T)/CBS levels; T1 diagnostic for CCSD(T) calculations; comparison of the calculated thermodynamic property with available experiment data; and CCSD(T)/CBS-VTST calculation procedure (PDF)

■ AUTHOR INFORMATION

Corresponding Authors

Yun Li − *School of Metallurgy and Environment, Central South University, Hunan Province, Changsha 410083, China*; Email: li.yun@csu.edu.cn

Jie Li − *School of Metallurgy and Environment, Central South University, Hunan Province, Changsha 410083, China; National Engineering Laboratory of High Efficient Recovery of Refractory Nonferrous Metals, Central South University, Hunan Province, Changsha 410083, China*; Email: 15773126138@163.com

Authors

Tianshuang Li − *School of Metallurgy and Environment, Central South University, Hunan Province, Changsha 410083, China; National Engineering Laboratory of High Efficient Recovery of Refractory Nonferrous Metals, Central South University, Hunan Province, Changsha 410083, China*; orcid.org/0000-0003-0081-4269

Hongliang Zhang − *School of Metallurgy and Environment, Central South University, Hunan Province, Changsha 410083, China; National Engineering Laboratory of High Efficient Recovery of Refractory Nonferrous Metals, Central South University, Hunan Province, Changsha 410083, China*; orcid.org/0000-0003-2878-8138

Jingkun Wang − *China Hongqiao Group Limited, Zouping 256200, China*

Jin Xiao − *School of Metallurgy and Environment, Central South University, Hunan Province, Changsha 410083, China; National Engineering Laboratory of High Efficient Recovery of Refractory Nonferrous Metals, Central South University, Hunan Province, Changsha 410083, China*

https://doi.org/10.1021/acsomega.1c02155
ACS Omega 2021, 6, 20471−20482

Complete contact information is available at:
https://pubs.acs.org/10.1021/acsomega.1c02155

Notes

The authors declare no competing financial interest.

■ ACKNOWLEDGMENTS

This work was financially supported by the National Natural Science Foundation of China (nos. 51974373 and 51874365), the Major Scientific and Technological Innovation Projects of Shandong Province (no. 2019JZZY020123), the China National Postdoctoral Program for Innovation Talents (no. BX20200391), and the Natural Science Foundation of Hunan Province, China (no. 2018JJ2521).

■ REFERENCES

(1) Statistical Review of World Energy, 2020, 69th ed., *BP p.l.c.*, https://www.bp.com (accessed 2021-02-20).
(2) Argyle, M. D.; Bartholomew, C. H. Heterogeneous catalyst deactivation and regeneration: A review. *Catalysts* **2015**, *5*, 145−269.
(3) Saleh, T. A. Characterization, determination and elimination technologies for sulfur from petroleum: Toward cleaner fuel and a safe environment. *Trends Environ. Anal.* **2020**, *25*, No. e00080.
(4) Demirbas, A.; Alidrisi, H.; Balubaid, M. A. API gravity, sulfur content, and desulfurization of crude oil. *Pet. Sci. Technol.* **2015**, *33*, 93−101.
(5) Sikarwar, P.; Gosu, V.; Subbaramaiah, V. An overview of conventional and alternative technologies for the production of ultra-low-sulfur fuels. *Rev. Chem. Eng.* **2019**, *35*, 669−705.
(6) Babich, I. V.; Moulijn, J. A. Science and technology of novel processes for deep desulfurization of oil refinery streams: A review. *Fuel* **2003**, *82*, 607−631.
(7) Song, C.; Hsu, C. S.; Mochida, I. *Chemistry of Diesel Fuels*; 1st ed.; Song, C.; Hsu, C. S.; Mochida, I.; Eds.; CRC Press, 2000.
(8) Link, D. D.; Baltrus, J. P.; Rothenberger, K. S.; Zandhuis, P.; Minus, D. K.; Striebich, R. C. Class- and structure-specific separation, analysis, and identification techniques for the characterization of the sulfur components of JP-8 aviation fuel. *Energy Fuels* **2003**, *17*, 1292−1302.
(9) Hsu, C. S.; Robinson, P. R. Gasoline Production and Blending. In *Springer Handbook of Petroleum Technology*; Hsu, C. S., Eds.; Springer: New York, 2017; pp 551−616.
(10) European Parliament. *Directive 2009/30/EC n.d.* https://eur-lex.europa.eu/legal-content/EN/TXT/?uri=CELEX%3A32009L0030&qid=1618062478760 (accessed 2021-04-10).
(11) United States Environmental Protection Agency. *Gasoline Standards n.d.* https://www.epa.gov/gasoline-standards/gasoline-sulfur (accessed 2021-04-10).
(12) Li, C.; Li, D.; Zou, S.; Li, Z.; Yin, J.; Wang, A.; Cui, Y.; Yao, Z.; Zhao, Q. Extraction desulfurization process of fuels with ammonium-based deep eutectic solvents. *Green Chem.* **2013**, *15*, 2793−2799.
(13) Song, C. An overview of new approaches to deep desulfurization for ultra-clean gasoline, diesel fuel and jet fuel. *Catal. Today* **2003**, *86*, 211−263.
(14) Song, C.; Ma, X. New design approaches to ultra-clean diesel fuels by deep desulfurization and deep dearomatization. *Appl. Catal., B* **2003**, *41*, 207−238.
(15) Kim, J. H.; Ma, X.; Zhou, A.; Song, C. Ultra-deep desulfurization and denitrogenation of diesel fuel by selective adsorption over three different adsorbents: A study on adsorptive selectivity and mechanism. *Catal. Today* **2006**, *111*, 74−83.
(16) Zhang, L.; Wang, J.; Sun, Y.; Jiang, B.; Yang, H. Deep oxidative desulfurization of fuels by superbase-derived Lewis acidic ionic liquids. *Chem. Eng. J.* **2017**, *328*, 445−453.
(17) Xiong, J.; Zhu, W.; Li, H.; Yang, L.; Chao, Y.; Wu, P.; Xun, S.; Jiang, W.; Zhang, M.; Li, H. Carbon-doped porous boron nitride: Metal-free adsorbents for sulfur removal from fuels. *J. Mater. Chem. A* **2015**, *3*, 12738−12747.
(18) Shi, Y.; Liu, G.; Wang, L.; Zhang, X. Efficient adsorptive removal of dibenzothiophene from model fuel over heteroatom-doped porous carbons by carbonization of an organic salt. *Chem. Eng. J.* **2015**, *259*, 771−778.
(19) Yang, R. T.; Maldonado, A.; Yang, F. H. Desulfurization of transportation fuels with zeolites under ambient conditions. *Science* **2003**, *301*, 79−81.
(20) Bianchini, C.; Meli, A. Hydrogenation, hydrogenolysis, and desulfurization of thiophenes by soluble metal complexes: Recent achievements and future directions. *Acc. Chem. Res.* **1998**, *31*, 109−116.
(21) Hua, R.; Wang, J.; Kong, H.; Liu, J.; Lu, X.; Xu, G. Analysis of sulfur containing compounds in crude oils by comprehensive two dimensional gas chromatography with sulfur chemiluminescence detection. *J. Sep. Sci.* **2004**, *27*, 691−698.
(22) Wang, M.; Zhao, S.; Chung, K. H.; Xu, C.; Shi, Q. Approach for selective separation of thiophenic and sulfidic sulfur compounds from petroleum by methylation/demethylation. *Anal. Chem.* **2015**, *87*, 1083−1088.
(23) Hana, Y.; Zhang, Y.; Xu, C.; Hsu, C. S. Molecular characterization of sulfur-containing compounds in petroleum. *Fuel* **2018**, *221*, 144−158.
(24) Wang, M.; Zhao, S.; Ren, L.; Han, Y.; Xu, C.; Chung, K. H.; Shi, Q. Refractory Cyclic Sulfidic Compounds in Deeply Hydrodesulfurized Diesels. *Energy Fuels* **2017**, *31*, 3838−3842.
(25) Xing, M.; Kong, J.; Dong, J.; Li, F. Thiophenic Sulfur Compounds Released During Coal Pyrolysis. *Environ. Eng. Sci.* **2013**, *30*, 273−279.
(26) Zhang, Y.; Han, Y.; Wu, J.; Wang, Y.; Li, J.; Shi, Q.; Xu, C.; Hsu, C. S. Comprehensive composition, structure, and size characterization for thiophene compounds in petroleum using ultrahigh-resolution mass spectrometry and trapped ion mobility spectrometry. *Anal. Chem.* **2021**, *93*, 5089−5097.
(27) Brunet, S.; Mey, D.; Perot, G.; Bouchy, C. I.; Diehl, F. On the hydrodesulfurization of FCC gasoline: a review. *Appl. Catal., A* **2005**, *278*, 143−172.
(28) Chandreyee, S.; Eric, L. T. Hydrodesulfurization of athabasca fluid coke conversion and mechanism. *Can. J. Chem. Eng.* **1995**, *73*, 211−219.
(29) Wynberg, H.; Bantjes, A. Pyrolysis of thiophene. *J. Org. Chem.* **1959**, *24*, 1421−1423.
(30) Cullis, C. F.; Norris, A. C. The pyrolysis of organic compounds under conditions of carbon formation. *Carbon* **1972**, *10*, 525−537.
(31) Winkler, J. K.; Karow, W.; Rademacher, P. Gas-phase pyrolysis of heterocyclic compounds, part 1 and 2: Flow pyrolysis and annulation reactions of some sulfur heterocycles: Thiophene, benzo[*b*]thiophene, and dibenzothiophene. A product-oriented study. *J. Anal. Appl. Pyrolysis* **2002**, *62*, 123−141.
(32) Memon, H. R. R.; Williams, A.; Williams, P. T. Shock tube pyrolysis of thiophene. *Int. J. Energy Res.* **2003**, *27*, 225−239.
(33) Hore, N. R.; Russell, D. K. The thermal decomposition of 5-membered rings: A laser pyrolysis study. *New J. Chem.* **2004**, *28*, 606−613.
(34) Vasiliou, A. K.; Hu, H.; Cowell, T. W.; Whitman, J. C.; Parish, C. A. Modeling oil shale pyrolysis: High-temperature unimolecular decomposition pathways for thiophene. *J. Phys. Chem. A* **2017**, *121*, 7655−7666.
(35) Huang, C.; Zhang, J.; Chen, J. Quantum chemistry study on the pyrolysis of thiophene functionalities in coal. *Coal Convers.* **2005**, *28*, 33−35.
(36) Ling, L.; Zhang, R.; Wang, B.; Xie, K. C. Density functional theory study on the pyrolysis mechanism of thiophene in coal. *J. Mol. Struct.* **2009**, *905*, 8−12.
(37) Song, X.; Parish, C. A. Pyrolysis mechanisms of thiophene and methylthiophene in asphaltenes. *J. Phys. Chem. A* **2011**, *115*, 2882−2891.

(38) Frisch, M. J.; Trucks, G. W.; Schlegel, H. B.; et al. *Gaussian 09*, Revision D01; Gaussian, Inc.: Wallingford, CT, 2009.
(39) Gonzalez, C.; Schlegel, H. B. Reaction path following in mass-weighted internal coordinates. *J. Phys. Chem.* **1990**, *94*, 5523−5527.
(40) Lee, T. J.; Taylor, P. R. A diagnostic for determining the quality of single-reference electron correlation methods. *Int. J. Quantum Chem.* **1989**, *S23*, 199−207.
(41) Lu, T.; Chen, Q. *Shermo*: A general code for calculating molecular thermodynamic properties. *ChemRxiv*, 2020. 10.26434/chemrxiv.12278801
(42) Grimme, S. Supramolecular binding thermodynamics by dispersion-corrected density functional theory. *Chem. - Eur. J.* **2012**, *18*, 9955−9964.
(43) Helgaker, T.; Klopper, W.; Koch, H.; Noga, J. Basis-set convergence of correlated calculations on water. *J. Chem. Phys.* **1997**, *106*, No. 9639.
(44) Neese, F.; Hansen, A.; Liakos, A. Efficient and accurate approximations to the local coupled cluster singles doubles method using a truncated pair natural orbital basis. *J. Chem. Phys.* **2009**, *131*, No. 064103.
(45) Li, T.; Li, J.; Zhang, H.; Yang, S.; Wang, J.; Xiao, J. Theoretical study on COS oxidation mechanism. *Combust. Flame* **2020**, *221*, 311−325.
(46) Li, T.; Li, J.; Zhang, H.; Sun, K.; Xiao, J. DFT research on benzothiophene pyrolysis reaction mechanism. *J. Phys. Chem. A* **2019**, *123*, 796−810.
(47) Li, T.; Li, J.; Zhang, H.; Sun, K.; Xiao, J. DFT study on the dibenzothiophene pyrolysis mechanism in petroleum. *Energy Fuels* **2019**, *33*, 8876−8895.
(48) Li, T.; Li, J.; Zhang, H.; Yang, S.; Wang, J.; Xiao, J. CBS-QB3 study on the pyrolysis mechanism of 3-ethynylebenzo[*b*] thiophene. *Chem. Phys. Lett.* **2021**, *762*, No. 138120.
(49) Goos, E.; Burcat, A.; Ruscic, B. *Third Millennium Ideal Gas and Condensed Thermochemical Database for Combustion*, 2010. http://garfield.chem.elte.hu/Burcat/hf.doc (accessed 2021-04-10).
(50) Barckholtz, C.; Barckholtz, T. A.; Hadad, C. M. C-H and N-H bond dissociation energies of small aromatic hydrocarbons. *J. Am. Chem. Soc.* **1999**, *121*, 491−500.
(51) Sendt, K.; Bacskay, G. B.; Mackie, J. C. Pyrolysis of furan: Ab initio quantum chemical and kinetic modeling studies. *J. Phys. Chem. A* **2000**, *104*, 1861−1875.
(52) Tian, Z.; Yuan, T.; Fournet, R.; Glaude, P.-A.; Sirjean, B.; Leclerc, F. B.; Zhang, Ku.; Qi, F. An experimental and kinetic investigation of premixed furan/oxygen/argon flames. *Combust. Flame* **2011**, *158*, 756−773.
(53) Hurley, C. D.; The pyrolysis of thiophene and related free-radical reactions. *Ph.D. Thesis*, The University of Surrey, 1979. http://epubs.surrey.ac.uk/847547/1/10798568.pdf (accessed 2021-04-10).

https://doi.org/10.1021/acsomega.1c02155
ACS Omega 2021, 6, 20471−20482